X-ray Absorption Spectromicroscopy Study of UV-Photoinduced Surface Modification and Anisotropy in Polyimide Films

M. Zharnikov,*,† Y. Ouchi,‡ M. Hasegawa,§ and A. Scholl||

Angewandte Physikalische Chemie, Universität Heidelberg, 69120 Heidelberg, Germany, Department of Chemistry, Nagoya University, Nagoya, 464-8602 Japan, IBM Research, Tokyo Research Laboratory, Yamato, Kanagawa 242-8502, Japan, and Advanced Light Source, Lawrence Berkeley National Lab, Berkeley, California 94720

Received: June 24, 2003; In Final Form: September 11, 2003

X-ray absorption spectromicroscopy with an X-ray photoelectron emission microscope (X-PEEM) was applied to study the modification of polyimide films by linear polarized deep ultraviolet (LPDUV) light, using LPDUV-patterned (0.4−1 J/cm^2) CBDA-ODA samples as a test system. Stacks of successive X-PEEM images were collected in the total electron yield acquisition mode over the photon energy ranges containing the relevant C, N, and O K-edges. The LPDUV-induced patterns could be clearly distinguished in the images acquired at the excitation energies of characteristic absorption resonances. The analysis of these images and the derived NEXAFS microspectra suggests that the LPDUV irradiation causes an anisotropic decomposition of the PI backbone with the cleavage of the cyclobutane ring to form a maleimide structure as the main decomposition channel. Whereas the UV-induced anisotropy was not directly perceptible in the X-PEEM images acquired at the excitation energies of characteristic absorption resonances, it could be clearly seen and evaluated in the corresponding microspectra. In particular, the dichroic ratio of the π(C═O*) resonance of imide was found to be ≈6%, in good agreement with previous spectroscopic results.

1. Introduction

The utilization of flat panel displays (FPD) has grown steadily over recent years, entering such new areas as home entertainment technology. A key element of these devices is a nematic liquid crystal (LC), which consists of an array of aligned rodlike molecules building a 90° twisted helix-like structure between two crossed polarizers. The twisted LC structure rotates the polarization direction of the transmitted linearly polarized light, so that it comes through the second polarizer and makes a bright spot on the FPD screen. By applying a small voltage from an electrode, the helical LC structure can be distorted so that no rotation of the light polarization occurs, which results in a dark spot on FPD screen. Taking an array of microscopic ITO electrodes independently driven by the corresponding thin-film transistor assembly, an image is formed pixel by pixel.

The 90° twist of LC molecules is achieved by the alignment of the outer constituents of the array (parallel to the polarization axes of the polarizers) at the electrode−LC interfaces. This alignment is usually mediated by thin polyimide (PI) films covering the ITO electrodes (see e.g. ref 1), although recently other substrate materials have been introduced.[2] The surface of these films is specially processed to gain an uniaxial anisotropy, which is subsequently "transmitted" to LC. The mechanism of the LC alignment has been debated over the last two decades,[1−13] but a general phenomenological theory was developed only recently.[1,10] This theory assumes that LC alignment results from a molecular interaction between the rodlike LC molecules and aligned polymer chains at the polyimide surface.[1]

A conventional way to introduce a uniaxial anisotropy into a PI surface is through unidirectional rubbing with a rotating drum whose surface consists of velour bristles. It has been proved experimentally that such a procedure causes the desired alignment of PI chains, which subsequently results in the desired orientation of the molecular orbitals responsible for the coupling of the LC constituents.[1,14−17] A correlation between the introduced asymmetry of the molecular bond and the LC alignment, including the so-called pre-tilt angle, has been demonstrated.[1]

Along with efforts to improve the technologically important rubbing method, much work has been devoted to the development of new approaches to introduce a uniaxial anisotropy into the PI surface. Among these approaches, ion beam irradiation under a grazing angle[18] and irradiation with linearly polarized UV light[19−25] are the most promising ones. Within the latter approach, photoisomerization,[19] photopolymerization,[20] and photodecomposition[22] of PI have been exploited to gain a uniaxial anisotropy, which allows alignment of the adjacent LC films. While photoisomerization and photopolymerization rely on specific materials, photodecomposition can utilize a wide range of PI compounds, and this potential has stimulated extensive research into the mechanism of LC alignment on photodecomposed PI surfaces.[22,24,25] It has been demonstrated that linearly polarized deep UV (LPDUV) light preferentially decomposes polymer chains that are parallel to its polarization direction, and LC molecules align perpendicularly to this direction.[24,25]

Recently, we performed an extensive study of UV-photoinduced surface anisotropy of PI by near-edge absorption fine structure (NEXAFS) spectroscopy both in the partial (PEY) and

* To whom correspondence should be addressed. Address: APC, Universität Heidelberg, Im Neuenheimer Feld 253, 69120, Heidelberg, Germany. Phone:+49-6221-544921. Fax: +49-6221-546199. E-mail: Michael.Zharnikov@urz.uni-heidelberg.de.

† Universität Heidelberg.

‡ Nagoya University.

§ Tokyo Research Laboratory.

|| Lawrence Berkeley National Lab.

10.1021/jp030782t CCC: $27.50
Published on Web 12/20/2003

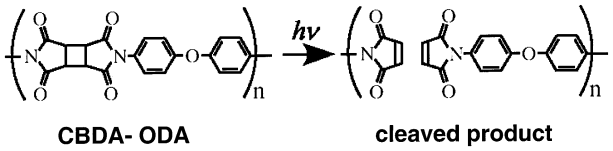

Figure 1. Molecular structure of CBDA-ODA and its assumed cleaved product.

total (TEY) electron yield acquisition mode,[26] which have a different depth sensitivity due to the different contributions of the inelastically scattered electrons in the acquired signal.[27] The degree of azimuthal alignment was estimated on the basis of the intensity variation of the $\pi^*_{C=O}$ resonance at the O K-edge. This parameter exhibited a characteristic dependence on the LPDUV exposure time: it reached its maximum value at low irradiation doses and decreased drastically with progressive irradiation, demonstrating the transition from anisotropic bond scission to isotropic damage. The maximum anisotropy was obtained at a UV exposure of 0.6 J/cm^2 (≈10%) and 4 J/cm^2 (≈8.3%) for the PEY and TEY acquisition modes, respectively. This difference implies that the film possesses the depth dependence of the anisotropy, so that the maximum alignment occurs in the vicinity of the film surface. The irradiation dependence of PEY-derived anisotropy and the order parameter of LC showed good agreement, in accordance with the current phenomenological theory of LC alignment (see above).

In this study, we used NEXAFS spectromicroscopy to visualize the LPDUV-induced modification of PI films and to investigate anisotropy in the near-surface area. A parallel goal was to demonstrate the applicability of X-ray absorption spectromicroscopy for studying the above-mentioned phenomena. Up to now, this technique has been applied exclusively to the rubbed PI surfaces,[28] which made it possible to image the assumed alignment of molecular orbitals and make some quantitative estimates for optimizing the rubbing procedure. Generally, NEXAFS spectromicroscopy can be successfully utilized to image the molecular orientation in polymers[29,30] and monomolecular films.[31,32]

2. Experimental Section

The UV-sensitive PI sample used was poly[4,4′-oxydiphenylene-1,2,3,4-cyclobutanetetra-carboximide] (CBDA-ODA), as shown in the left part of Figure 1.[24,25,33] UV light irradiation is assumed to cleave the cyclobutane ring in the PI backbone to form a maleimide structure as illustrated in the right part of Figure 1. Precursor polyamic acid of CBDA-ODA dissolved in butyl cellosolve was spin-coated onto indium−tin-oxide-coated glass plates and imidized at 250 °C for 1 h, which resulted in a homogeneous film with a thickness of less than 200 nm. The LPDUV irradiation of the PI films was performed through a mask with a 10 μm square opening and 5 μm stripes. LPDUV light (257 nm, 15 mW/cm^2) was provided by a frequency-doubled Ar^+ laser (514 nm). The LPDUV exposure was 0.4 and 1.0 J/cm^2.

The experiments were conducted at a microscopy branch (7.3.1.1) of the beamline 7.3.1 at the Advanced Light Source in Berkeley, CA. This branch operates over the photon energy range from 175 to 1500 eV with a spectral resolving power between 1000 and 2000. It is equipped with an X-ray photoelectron emission microscope (X-PEEM), which operates in the TEY acquisition mode and provides a spatial resolution of typically 50−100 nm for elemental contrast imaging.

Stacks of successive NEXAFS images over the photon energy ranges containing the relevant C, N, and O K-edges were acquired in the grazing incidence geometry. The measurements were performed using linearly polarized soft X-rays with the electric field vector, $\mathbf{E}_{SX}$, being either parallel ($\mathbf{E}_{SX} \parallel \mathbf{E}_{UV}$) or perpendicular ($\mathbf{E}_{SX} \perp \mathbf{E}_{UV}$) to the polarization axis of the LPDUV light, $\mathbf{E}_{UV}$. Special care was taken to avoid X-ray damage, because the observed contrasts disappeared after only 10−20 s of exposure to the X-ray flux at the standard settings of the beamline. The necessary steps included minimizing openings for the beamline slits, putting a Ti foil into the light track, and using an aperture to restrict the illuminated area. These steps allowed us to increase the "life time" of the LPDUV-induced structures to 5−10 min, which was sufficient to acquire an individual image stack.

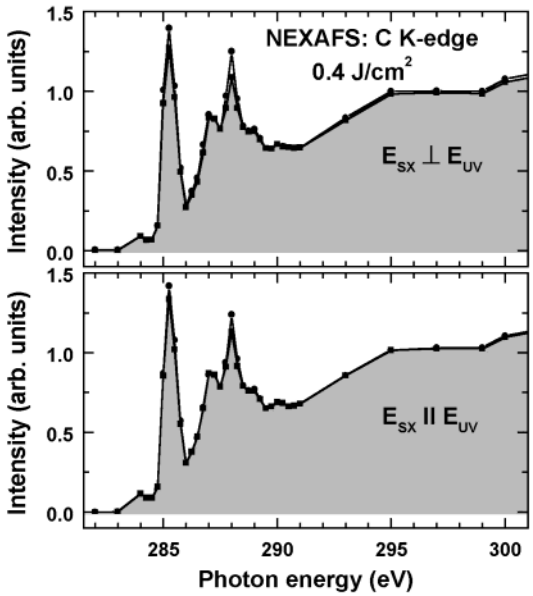

Figure 2. Normalized C K-edge NEXAFS microspectra from pristine and LPDUV-irradiated (shadowed) areas of CBDA-ODA for $\mathbf{E}_{SX} \perp \mathbf{E}_{UV}$ (upper panel) and $\mathbf{E}_{SX} \parallel \mathbf{E}_{UV}$ (lower panel). The X-PEEM imaging was performed at fixed photon energies marked by circles and squares for pristine and irradiated areas, respectively.

By integrating over selected areas of the collected images, the C, N, and O K-edge NEXAFS microspectra were derived for both the LPDUV-irradiated and pristine regions. A conventional normalization procedure was applied, including normalizing the raw spectra to the monochromator transmission, subtracting the preedge signal, and scaling the edge jump to get an intensity of unity at 35−40 eV above the absorption edge.[34]

The images acquired at the absorption resonance positions were normalized to the noncontrast images acquired far from the absorption edge. This procedure significantly improved the observed contrasts and eliminated the effects related to a nonhomogeneous illumination of the field of view by the incoming X-ray beam.

3. Results

Normalized C, N, and O K-edge NEXAFS microspectra for pristine and LPDUV-irradiated (shadowed) areas of CBDA-ODA are presented in Figures 2−4, respectively. The upper and lower panels correspond, respectively, to the $\mathbf{E}_{SX} \perp \mathbf{E}_{UV}$ and $\mathbf{E}_{SX} \parallel \mathbf{E}_{UV}$ experimental geometries. These spectra were derived from the stacks of the X-PEEM images acquired at fixed photon energies, marked by circles and squares in Figures 2−4. For example, raw NEXAFS images of LPDUV-patterned CBDA-ODA recorded at the position of the π (C*═O)

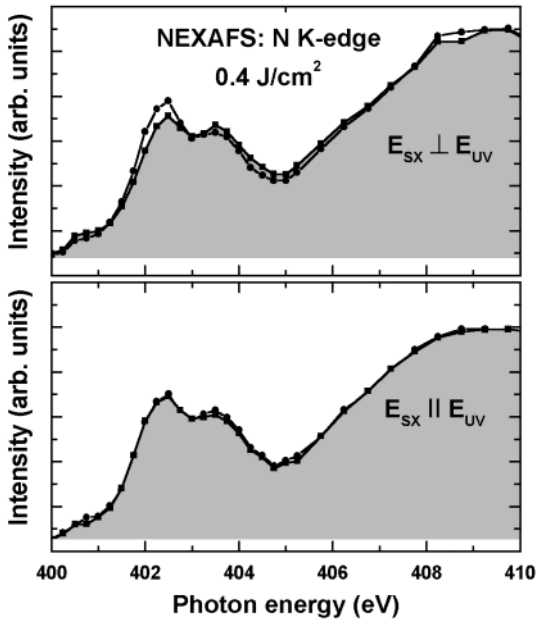

Figure 3. Normalized N K-edge NEXAFS microspectra from pristine and LPDUV-irradiated (shadowed) areas of CBDA-ODA for $\mathbf{E}_{SX} \perp \mathbf{E}_{UV}$ (upper panel) and $\mathbf{E}_{SX} \parallel \mathbf{E}_{UV}$ (lower panel). The X-PEEM imaging was performed at fixed photon energies marked by circles and squares for pristine and irradiated areas, respectively.

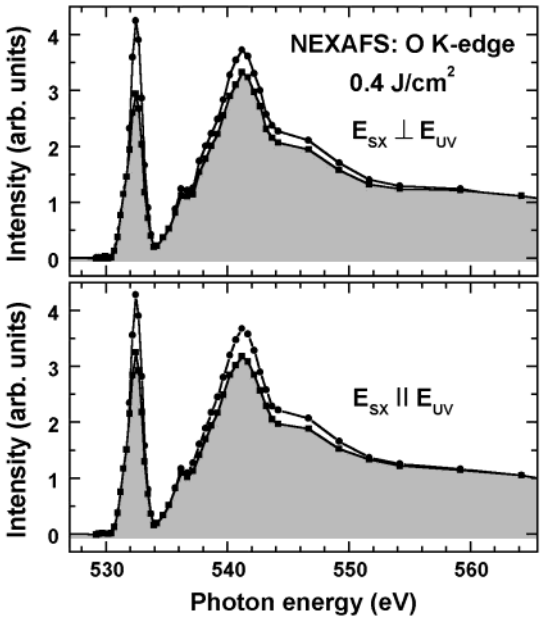

Figure 4. Normalized O K-edge NEXAFS microspectra from pristine and LPDUV-irradiated (shadowed) areas of CBDA-ODA for $\mathbf{E}_{SX} \perp \mathbf{E}_{UV}$ (upper panel) and $\mathbf{E}_{SX} \parallel \mathbf{E}_{UV}$ (lower panel). The X-PEEM imaging was performed at fixed photon energies marked by circles and squares for pristine and irradiated areas, respectively.

resonance (287.9 eV) and far above the absorption edge (299 eV) are presented at the left and center of Figure 5, along with the respective normalized π (C*═O) image (at the right).

The normalized NEXAFS microspectra accurately represent the intensity relation between the pristine and LPDUV-irradiated areas of the raw images. This relation is not distorted by the spectra normalization procedure, which is proven by the complete correlation between the observed intensity differences in the normalized spectra and the respective raw images: the LPDUV-induced pattern is only perceptible at the photon energies at which there is a noticeable intensity difference in

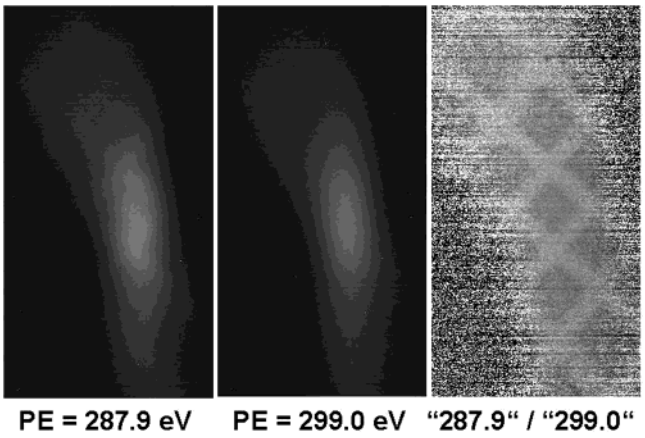

Figure 5. As-measured X-PEEM images of LPDUV-patterned CBDA-ODA recorded at 287.9 eV ($\pi^*_{C=O}$) and 299 eV (far above the absorption resonances), along with the respective normalized image (the image at 287.9 eV divided by the image at 299 eV). The LPDUV-induced pattern is perceptible (even though with a low contrast) in the raw π (C*═O) image and becomes clearly visible after normalization to the background image (299 eV), which does not exhibit any contrast. The size of the irradiated squares is 10×10 μm^2.

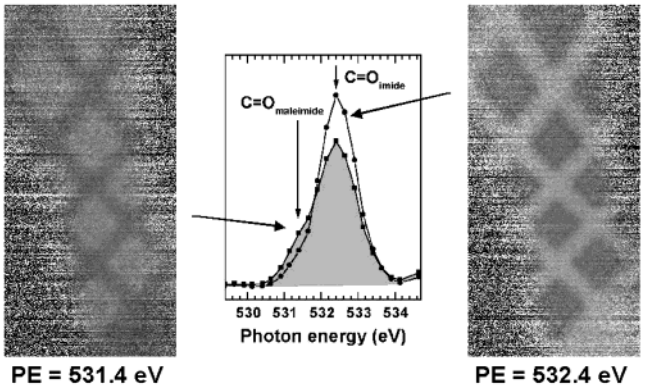

Figure 6. Normalized X-PEEM images of LPDUV-patterned CBDA-ODA recorded at 531.4 eV ($\pi^*_{C=O}$ for maleimide) and 532.4 eV ($\pi^*_{C=O}$ for imide), along with the respective O K-edge NEXAFS microspectra from nonirradiated and UV-irradiated (shadowed) areas. The images were normalized to the images for the postedge excitation region (566 eV), which did not reveal any contrast. The size of the irradiated squares is 10×10 μm^2.

the normalized spectra. As seen in Figures 2−4, this difference is only observed at the positions of characteristic absorption resonances, such as π* resonances for phenyl (285.2 eV) and carbonyl (287.9 eV) carbon in the C K-edge spectra; two closely placed π*-like resonances at 402.5 and 403.5 eV in the N K-edge spectra; and π(C═O*) resonances for maleimide (531.4 eV) and imide (532.4 eV) and σ(C═O*) resonances at 541.3 and 546.5 eV in the O K-edge spectra (the assignment for maleimide is based on our theoretical calculations).[35] The observed contrast in the X-PEEM images exactly follows the intensity relation between the absorption resonance intensities. In particular, the pristine areas of CBDA-ODA in the normalized π (C*═O) image in Figure 5 exhibit a higher TEY intensity than the LPDUV-irradiated ones, in agreement with a higher intensity of the π (C*═O) resonance for pristine CBDA-ODA in the C K-edge spectra in Figure 2. Another example is given by Figure 6, where the normalized X-PEEM images of LPDUV-patterned CBDA-ODA recorded at 531.4 eV ($\pi^*_{C=O}$ for maleimide) and 532.4 eV ($\pi^*_{C=O}$ for imide) are presented along with an extract from the respective micro-NEXAFS O K-edge spectra of nonirradiated and LPDUV-irradiated (shadowed) areas

(Figure 4). Both in the spectra and in the images, the pristine areas of CBDA-ODA exhibit a higher $\pi^*_{C=O}$ resonance intensity for imide and a lower $\pi^*_{C=O}$ resonance intensity for maleimide than the LPDUV-irradiated areas do. In general, both the normalized NEXAFS spectra and the respective raw and normalized images comprise a fully consistent data set representing the real intensity distributions in the LPDUV-patterned CBDA-ODA.

Although the intensity differences between the pristine and LPDUV-irradiated areas are observed for both $\mathbf{E}_{SX} \perp \mathbf{E}_{UV}$ and $\mathbf{E}_{SX} \parallel \mathbf{E}_{UV}$, the extent of the LPDUV-induced changes is larger for the former orientation, as seen in the normalized spectra in Figures 2−4. Taking the dichroic ratio D in the same way as in ref 26

$$D = [I(\mathbf{E}_{SX} \parallel \mathbf{E}_{UV}) - I(\mathbf{E}_{SX} \perp \mathbf{E}_{UV})]/[I(\mathbf{E}_{SX} \parallel \mathbf{E}_{UV}) + I(\mathbf{E}_{SX} \perp \mathbf{E}_{UV})] \quad (1)$$

we get a values of ≈3% for the π^*(phenyl) resonance, ≈4.5% for the π(C*═O) resonance, ≈7% for the π^* resonances at the N K-edge, and ≈6% for the π(C═O*) resonance for imide (the errors of these values are 10−20%). The last estimate is in good agreement with the analogous value from ref 26 (7−7.5% at a LPDUV exposure of 0.2−1 J/cm^2). Note that the exact comparison of dichroic ratios derived from different experimental setups requires a correction factor $1/(2P - 1)$,[16,28] where P is the polarization degree of the synchrotron light.

The LPDUV-induced dichroism is practically imperceptible in the X-PEEM images: if the photon energy is fixed, the images acquired at $\mathbf{E}_{SX} \perp \mathbf{E}_{UV}$ and $\mathbf{E}_{SX} \parallel \mathbf{E}_{UV}$ exhibit similar intensity distributions over the field of view, so that the information on the dichroism can only be obtained by a numerical evaluation of the corresponding microspectra, as was done above. Note that the intensity distribution in the X-PEEM images depends not only on the LPDUV-induced chemical changes but also on the intensity relation between the inelastic background and the relevant absorption resonance. In particular, the best contrast was observed at the position of the intense π(C═O*) resonance for imide, while the images acquired at the positions of the low-intense π^* resonances at the N K-edge exhibited a rather poor contrast, the LPDUV-induced pattern was hardly perceptible.

4. Discussion

The experimental data imply that the exposure of CBDA-ODA to LPDUV light results in an anisotropic decomposition of the polymer chains. The lack of a perceptible contrast in the X-PEEM images for the preedge and postedge photon energy regions suggests that the decomposition products do not desorb from the polymer surface but remain there. The observed intensity differences between the pristine and irradiated areas at the positions of the π^*(C*═O) and π^*(C═O*) resonances for imide and maleimide imply a cleavage of the cyclobutane ring in the CBDA-ODA backbone (leading to the formation of a maleimide structure) as the main pathway of the UV-induced decomposition, which is in full agreement with previous results.[26] Parallel decomposition channels are possible, e.g., as implied by the reduction of the π^*(phenyl) resonance intensity upon LPDUV irradiation. Additional information can probably be obtained from detailed analysis of the N K-edge NEXAFS spectra, which were collected for the first time (to our knowledge) for the anisotropic PI surface. For such an analysis, exact assignment of the relevant π^*-like resonances is desirable but is unfortunately not available. The resonance at 402.5 eV can be tentatively assigned to the π^* orbital of imide,[36] which is a reasonable conclusion considering that this resonance behaves like the π^*(C═O*) resonance for imide in the O K-edge spectra.

The UV-induced anisotropy was not directly perceptible in the X-PEEM images acquired at the positions of the absorption resonances but was detectable in the extracted microspectra, which could also be quantitatively evaluated. The dichroic ratio for the π(C═O*) resonance of imide was estimated to be ≈6%, which is in good agreement with a value of 7−7.5% obtained from an analysis of O K-edge NEXAFS spectra of CBDA-ODA exposed to 0.2−1 J/cm^2 of LPDUV.[26] The dichroic ratios for the other absorption resonances cannot be compared to previous values, as no spectroscopic measurements for LPDUV-irradiated CBDA-ODA have been performed at the C and N K-edges. However, the dichroic ratios for the π^*(phenyl) and π(C*═O) resonances can be compared with analogous values obtained for the rubbed PI on the basis of the evaluation of C K-edge NEXAFS[16] and micro-NEXAFS[28] spectra. The latter values were estimated to be 20−21%, which is noticeably higher than the values of 3% for the π^*(phenyl) resonance and ≈4.5% for the π(C*═O) resonance obtained in this study. Nevertheless, even this small dichroism is enough to achieve a suitable alignment of LC, as was precisely demonstrated in ref 26. Note that the LPDUV-induced anisotropy at the surface of CBDA-ODA is somewhat higher than has been estimated from the presented TEY microspectra, which are not as surface-representative as PEY and AEY data. The difference between the PEY-derived and TEY-derived dichroic ratio is especially large at a small LPDUV exposure (up to 2 J/cm^2)[26] and can achieve a factor of 1.5.[26]

5. Summary

NEXAFS spectromicroscopy with X-PEEM was proven to be a suitable technique to visualize and study LPDUV-induced modification of PI films, using CBDA-ODA as a test system and taking advantages of a direct comparison of the signal intensities for different sample areas. The measurements have been performed at all three relevant absorption edges, namely, the C, N, and O K-edges. LPDUV-induced patterns could be only distinguished in the X-PEEM images acquired at the excitation energies of characteristic absorption resonances. For the photon energies corresponding to the preedge and postedge ranges, no pattern was perceptible in the images, which suggests that the observed contrasts are not topographic or desorption-related ones, but rather indicate specific chemical changes in the LPDUV-irradiated CBDA-ODA.

Analysis of the X-PEEM images and the derived NEXAFS microspectra suggests that LPDUV irradiation causes an anisotropic decomposition of the PI backbone, with cleavage of the cyclobutane ring to form a maleimide structure as the main (but not exclusive one) decomposition channel. The decomposition products were found to do not desorb from the polymer surface, but remain there. While the UV-induced anisotropy was not directly perceptible in the X-PEEM images acquired at the excitation energies of characteristic absorption resonances, it could be clearly seen in the corresponding microspectra. The dichroic ratio was estimated as ≈3% for the π^*(phenyl) resonance, ≈4.5% for the π(C*═O) resonance, ≈7% for the π^* resonances at the N K-edge, and ≈6% for the π(C═O*) resonance of imide. Even though these values are noticeably lower than those for the rubbing procedure, they are large enough to achieve a suitable alignment of LC.

Acknowledgment. The authors are very grateful to Michael Grunze for his support. We thank Andrew Doran (ALS) for technical help. This work has been supported by the German BMBF (GRE1HD), the U.S. Department of Energy under Contract No. DE-AC03-76SF00098, and a Japanese Grant-in-Aid from MEXT (14GS0213).

References and Notes

(1) Stöhr, J.; Samant, M. G. *J. Electron. Spectrosc. Relat. Phenom.* **1999**, *98*−*99*, 189.
(2) Stöhr, J.; Samant, M. G.; Lüning, J.; Callegari, A. C.; Chaundhari, P.; Doyle, J. P.; Lacey, J. A.; Lien, S. A.; Purushothaman, S.; Speidell, J. L. *Science* **2001**, *292*, 2299.
(3) Berreman, D. W. *Phys. Rev. Lett.* **1972**, *28*, 1683; *Mol. Cryst. Liq. Cryst.* **1973**, *23*, 187.
(4) Okano, K.; Matsuura, N.; Kobayashi, S. *Jpn. J. Appl. Phys.* **1982**, *21*, L109.
(5) Okano, K. *Jpn. J. Appl. Phys.* **1983**, *22*, L343.
(6) Geary, J. M.; Goodby, J. W.; Kmetz, A. R.; Patel, J. S. *J. Appl. Phys.* **1987**, *62*, 4100.
(7) Mada, H.; Sonoda, T. *Jpn. J. Appl. Phys.* **1993**, *32*, L1245.
(8) Han, K. Y.; Uchida, T. *Proceedings Eurodisplay 1993*; SID: Strasbourg, France, 1993; pp 13−16.
(9) Johannsmann, D.; Zhou, H.; Sonderkaer, P.; Wierenga, H.; Myrvold, B. O.; Shen Y. R. *Phys. Rev. E* **1993**, *48*, 1889.
(10) Zhuang, X.; Marrucci, L.; Shen, Y. R. *Phys. Rev. Lett.* **1994**, *73*, 1513.
(11) Kobayashi, S.; Iimura, Y. *SPIE* **1994**, *2175*, 122.
(12) Toney, M. F.; Russel, T. P.; Logan, J. A.; Kikuchi, H.; Sands, J. M.; Kumar, S. K. *Nature* **1995**, *374*, 709.
(13) Zhuang, X.; Wilk, D.; Marruci, L.; Shen, Y. R. *Phys. Rev. Lett.* **1995**, *75*, 2144.
(14) Ouchi, Y.; Oji, H.; Sei, M.; Ito, E.; Araki, T.; Ishii, H.; Seki, K.; Kondo, K. *Physika B* **1995**, *208*−*209*, 407.
(15) Mori, I.; Araki, T.; Ishii, H.; Ouchi, Y.; Seki, K.; Kondo, K. *J. Electron. Spectrosc. Relat. Phenom.* **1996**, *78*, 371.
(16) Samant, M. G.; Stöhr, J.; Brown, H. R.; Russel, T. P.; Sands, J. M.; Kumar, S. K. *Macromolecules* **1996**, *29*, 8334.
(17) Weiss, K.; Wöll, Ch.; Böhm, E.; Fiebranz, B.; Forstmann, G.; Peng, B.; Scheumann, V.; Johannsmann, D. *Macromolecules* **1998**, *31*, 1930.
(18) Chaudhari, P.; Lacey, J.; Lien, A.; Speidell, J. *Jpn. J. Appl. Phys. Part 2 Lett.* **1998**, *37*, L55.
(19) Gibbons, W. M.; Shannon, P. J.; Sun, S. T.; Swetlin, B. J. *Nature* **1991**, *351*, 49.
(20) Schadt, M.; Schmitt, K.; Kozinkov, V. *Jpn. J. Appl. Phys.* **1992**, *31*, 2155.
(21) Shannon, P. J.; Gibbons, W. M.; Sun, S. T. *Nature* **1994**, *368*, 532.
(22) Hasegawa, M.; Taira, Y. J. *Photopolym. Sci. Technol.* **1995**, *8*, 241.
(23) Schadt, M.; Seiberle, H.; Schuster, A. *Nature* **1996**, *381*, 212.
(24) Sakamoto, K.; Usami, K.; Araya, T.; Ushioda, S. *Jpn. J. Appl. Phys.* **1999**, *38*, L1435.
(25) Hasegawa, M. *Jpn. J. Appl. Phys.* **1999**, *38*, L457.
(26) Matsuie, N.; Ouchi, Y.; Oji, H.; Ishii, H.; Seki, K.; Hasegawa, M.; Zharnikov, M. *Jpn. J. Appl. Phys.* **2003**, *42*, L67.
(27) Zharnikov, M.; Frey, S.; Heister, K.; Grunze, M. *J. Electron. Spectrosc. Relat. Phenom.* **2002**, *124*, 15.
(28) Cossy-Favre, A.; Diaz, J.; Liu, Y.; Brown, H. R.; Samant, M. G.; Stöhr, J.; Hanna, A. J.; Anders, S.; Russel, T. R. *Macromolecules* **1998**, *31*, 4957.
(29) Ade, H.; Hsiao, B. *Science* **1993**, *262*, 1427.
(30) Ade, H.; Smith, A. P.; Zhang, H.; Thuang, G. R.; Kirz, J.; Rightor, E.; Hitchcock, A. P. *J. Electron. Spectrosc. Relat. Phenom.* **1997**, *84*, 53.
(31) Zharnikov, M.; Neuber, M.; Grunze, M. *J. Electron. Spectrosc. Relat. Phenom.* **1999**, *98*−*99*, 25.
(32) Zharnikov, M.; Neuber, M. *Surf. Sci.* **2000**, *464*, 8.
(33) Nishikawa, M.; Taheri, B.; West, J. L. *App. Phys. Lett.* **1998**, *72*, 2403.
(34) Stöhr, J. *NEXAFS Spectroscopy*; Springer Series in Surface Science 25; Springer-Verlag: New York, 1992.
(35) Matsuie, N.; Ouchi, Y.; Oji, H.; Ishii, H.; Seki, K.; Hasegawa, M. in preparation for publication.
(36) Gölzhäuser, A.; Panov, S.; Schertel, A.; Mast, M.; Wöll, Ch.; Grunze, M. *Surf. Sci.* **1995**, *334*, 235.